



HAL
open science

Near Infrared labeling of PLGA for in vivo imaging of nanoparticles

Regina Reul, Nicolas Tsapis, Hervé Hillaireau, Lucie Sancey, Simona Mura, Marion Recher, Julien Nicolas, Jean-Luc Coll, Elias Fattal

► **To cite this version:**

Regina Reul, Nicolas Tsapis, Hervé Hillaireau, Lucie Sancey, Simona Mura, et al.. Near Infrared labeling of PLGA for in vivo imaging of nanoparticles. *Polymer Chemistry*, 2012, 3 (3), pp.694. 10.1039/c2py00520d . hal-04101322

HAL Id: hal-04101322

<https://hal.science/hal-04101322>

Submitted on 19 May 2023

HAL is a multi-disciplinary open access archive for the deposit and dissemination of scientific research documents, whether they are published or not. The documents may come from teaching and research institutions in France or abroad, or from public or private research centers.

L'archive ouverte pluridisciplinaire **HAL**, est destinée au dépôt et à la diffusion de documents scientifiques de niveau recherche, publiés ou non, émanant des établissements d'enseignement et de recherche français ou étrangers, des laboratoires publics ou privés.

Near Infrared labeling of PLGA for *in vivo* imaging of nanoparticles

Regina Reul^{1,2}, Nicolas Tsapis^{1,2*}, Hervé Hillaireau^{1,2}, Lucie Sancey^{3,4}, Simona Mura^{1,2}, Marion Recher^{1,2}, Julien Nicolas^{1,2}, Jean-Luc Coll^{3,4} and Elias Fattal^{1,2}

1- Univ Paris-Sud, UMR CNRS 8612, Faculté de Pharmacie, Châtenay-Malabry, France

2- CNRS, UMR 8612, Faculté de Pharmacie, Châtenay-Malabry, France

3- INSERM CRI UJF U823, Institut Albert Bonniot, Grenoble Cedex 9, France

4 – Université Joseph Fourier, Grenoble, France

*Corresponding author

Nicolas Tsapis

UMR CNRS 8612, Univ Paris-Sud

5, rue JB Clément

92296 Châtenay-Malabry

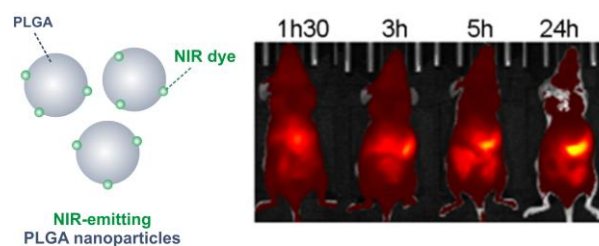
France

Tel 33 1 46 83 58 13

Fax 33 1 46 83 59 46

nicolas.tsapis@u-psud.fr

TOC



Near Infrared labeling of PLGA for *in vivo* imaging of nanoparticles

Abstract

To introduce optical imaging among methods available to follow nanoparticle biodistribution, we have evaluated the concept of covalently-labeling poly(lactide-*co*-glycolide) (PLGA) with a near-infrared (NIR) dye to obtain stable NIR fluorescent nanoparticles. PLGA was coupled with the NIR dye (DY-700, Dyomics) by an amide bond with 38% efficiency. Incorporating 1% of this conjugate into PLGA nanoparticles stabilised by polyvinyl alcohol (PVA) leads to stable nanoparticles (NPs) without affecting their colloidal characteristics (average diameter, polydispersity and zeta potential). In addition, nanoparticles remain strongly fluorescent and display good storage stability for 4 weeks at 4°C or over one week at 37°C. Nanoparticle cytotoxicity evaluated using HUVEC, NIH/3T3 and J774.A1 cell lines was similar for unlabeled or labeled NPs. Fluorescent nanoparticles and free dye were injected intravenously to mice and their biodistribution was followed during 24 h by NIR imaging, *in vivo* and *ex vivo*. Nanoparticles were found mainly in the liver whereas the free dye was not accumulating preferentially in this organ. The DY-700 NIR conjugate incorporated into PLGA NPs shows good performance both *in vitro* and *in vivo*, thus paving the way to finely traceable PLGA nanosystems for *in vivo* administration.

Keywords: PLGA, NIR imaging, covalently labeled conjugate, nanoparticles, biodistribution.

Introduction

Nanosystems such as nanoparticles (NPs) have been applied to the formulation of nanomedicine designed for controlled and targeted delivery of drugs as well as for diagnostic applications¹⁻³. Translation to the clinics will potentially improve drug therapeutic efficiency since nanomedicines reduce both drug side effects and toxicity⁴. However, the very same properties that make NPs exciting devices, might induce harmful effects as they interact with specific cells. NPs are solid colloidal systems smaller than 1 μm . Due to their small size, they exhibit a large specific surface area which makes their reactivity to biological systems very high and might consequently induce undesired effects and severe toxicities⁵. Most toxicity studies have been focusing on inorganic NPs: carbon nanotubes, fullerenes, urban particulate matter, silica and metal NPs⁶⁻⁸. The evaluation of nanomedicine toxicity has started to raise attention of the community but most studies still consider that due to their biodegradability, polymer NPs do not lead to side-effects or toxicity. However, previous results contrast with this general view: specific risks might arise from the nanoparticle form itself. For example, after intravenous administration, biodegradable poly(alkyl cyanoacrylate) NPs can trigger an inflammation and oxidative stress during both acute and chronic treatments⁹. However, this effect was reversible after interruption of the treatment while it was not the case for non-biodegradable polystyrene NPs. In order to study the potential toxicity of biodegradable NPs, it is crucial to follow their biodistribution and to check for undesired organ accumulation¹⁰⁻¹². Near infrared (NIR) optical imaging is as a powerful tool for *in vivo* experiments, being a minimally invasive, non-ionizing method allowing sensitive deep tissue imaging¹³. In monitoring applications in whole-body living tissue, the advantageous long emission of NIR is preferred, as most tissues generate little NIR fluorescence^{14, 15}. Labeling NPs with NIR moieties could be used to monitor the fate of NPs after administration. For biodegradable polymer NPs, although encapsulation of quantum dot has shown promising results¹⁶⁻¹⁹, covalent labeling has recently started to attract attention²⁰ since artifacts have been observed with dye encapsulation^{21, 22}.

Poly(lactide-co-glycolide) (PLGA), an FDA approved polymer, is the component of many biodegradable nanosystems^{2, 23-31}, however, covalent labeling with a NIR moiety has only been recently tested²⁰. Although the strategy we propose is based on the similar coupling chemistry, we report herein a comprehensive study in which surface properties, colloidal stability, label integrity, potential cytotoxicity, fluorescent properties as well as *in vivo* and *ex vivo* biodistributions following intravenous administrations were thoroughly detailed.(Scheme 1).

Materials and methods

Materials

Poly(lactide-*co*-glycolide) PLGA Resomer RG502 H (50:50 lactic to glycolic acid ratio, M_n 7900 g.mol⁻¹, M_w 14600 g.mol⁻¹) and PLGA Resomer RG756 S (75:25 lactic to glycolic acid ratio) were provided by Boehringer-Ingelheim (Germany). Polyvinyl alcohol (PVA) (MW 30000–70000 g.mol⁻¹, 89% hydrolyzed) was purchased from Sigma–Aldrich (France). The NIR label DY-700 amine was purchased from Dyomics (Dyomics, Germany). Solvents were obtained from Carlo Erba (Italy). Water was purified using a Synergy set-up from Millipore (France). Cell culture reagents such as DMEM (Dulbecco's modified Eagle's medium), RPMI 1640 (Roswell Park Memorial Institute medium), FBS (Fetal Bovine Serum), Trypsine-Versene (EDTA) and PBS (Ca²⁺ and Mg²⁺ free phosphate buffer) were purchased from Lonza (Belgium). All other chemicals of analytical grade were purchased from Sigma (Sigma Aldrich, France).

Synthesis of the DY-PLGA conjugate

Briefly, PLGA 502H was dissolved into dichloromethane (DCM) at a concentration of 0.01 mmol.mL⁻¹. 5.6 molar equivalents of *N,N'*-dicyclohexylcarbodiimide (DCC) with respect to PLGA and 5.6 molar equivalents of *N*-hydroxysuccinimide (NHS) predissolved into DCM (0.5 mmol.mL⁻¹) were then added. The reaction was maintained upon magnetic stirring at room temperature (20°C) until precipitation was observed and then for an additional hour. The solution was then filtered through a pipette tightly packed with cotton to remove the precipitated dicyclohexylurea (DCU). The production of DCU is indicative of successful activation of PLGA. The appropriate amount of PLGA-NHS was taken for the subsequent conjugation reaction. DY-700 amine was dissolved into a small amount of dimethylformamide (DMF) (0.027 mmol.mL⁻¹) in an amber vial, then one equivalent of PLGA-NHS in DCM was added, as well as 4 equivalents of triethylamine (TEA) diluted in DMF (0.13 mmol.mL⁻¹). The conjugation reaction was maintained upon magnetic stirring at room temperature (20°C) for 60 h. Finally, the mixture was precipitated into ice-cold methanol at a 1:10 volume ratio and centrifuged for 1 h at 4°C at 20000 rpm (maximum 37000 × g) using a Beckman Coulter Optima LE-80K ultracentrifuge (Beckman Coulter Inc., France). The precipitate was redissolved into DCM and the procedure was repeated three times more. To ensure its efficacy, purification was monitored by measuring the supernatants by fluorimetry to assess the presence of free dye. The conjugate was finally washed with methanol. DY-PLGA was protected from light continuously using amber glassware or aluminum foil. Labeling efficacy was measured by fluorimetry using an excitation wavelength of 700 nm and an emission wavelength of 725 nm in a mixture of DCM:ethanol 2:1 (v:v).

Nanoparticle preparation

NPs were prepared using a solvent emulsion evaporation method using PVA as stabilizer^{32, 33}. Briefly 25 mg of PLGA Resomer 756 were dissolved into 1.25 mL of a DCM:acetone (1:1 v:v) mixture. This organic solution was pre-emulsified by vortexing for 1 min with 5 mL of a pre-cooled 0.25 % (w/v) PVA aqueous solution (4°C). The pre-emulsion was kept on ice and sonicated for 1 minute using a VibraCell Sonicator (Fischer Scientific, Illkirch, France) at 40% of power. The organic phase was then evaporated at room temperature upon magnetic stirring (600 rpm) under a fume hood. To ascertain that the presence of the dye would not modify the nanoparticle surface chemistry, the NIR conjugate has been introduced in very small quantities (1% w/w) as compared with the work of Tosi *et al.*²⁰: 1% of DY-PLGA (w/w) was introduced into the formulation replacing 1% of PLGA Resomer 756. NPs were then purified by ultracentrifugation (maximum $37000 \times g$, 1 h, 4 °C, Beckman Coulter Optima LE-80 K, Beckman Coulter, Inc., France) to remove the excess of PVA. After centrifugation, NPs were redispersed at concentrations of 5 mg.mL⁻¹ and 25 mg.mL⁻¹ in water or in cell culture medium.

Size exclusion chromatography

Size exclusion chromatography (SEC) was performed at 30°C with two columns from Polymer Laboratories (PL-gel MIXED-D; 300 × 7.5 mm; bead diameter: 5 µm; linear part: 400 – 4 × 10 g.mol⁻¹) calibrated against PS standards in chloroform (CHCl₃) at a flow rate of 1 mL.min⁻¹. A SEC system equipped with a Waters 501 HPLC pump (Millipore, France), a waters 717 plus autosampler (Milipore France), a differential refractive index detector (Spectrasystem RI-150 from Thermo Electron Corp., France) and a UV detector (Waters 486 tunable absorbance detector, Milipore, France) was used.

Fluorescence measurements

Fluorescence was measured using a Perkin Elmer Luminescence Spectrometer LS50B (Perkin Elmer, France) and a 1 cm optical path cuvette. Fluorescence measurements were performed in DCM:ethanol 2:1 (v:v), in water or in rat serum fixing the excitation at 700 nm and collecting the emitted fluorescence at 725 nm.

Size and zeta potential

Average diameter and polydispersity index (PDI) were obtained using a Malvern Zetasizer Nano ZS (Malvern Instrument, UK) based on quasi-elastic light scattering. Size measurements were

performed at 20°C, at an angle of 173° to avoid multiple scattering. Zeta potential was measured using the same instrument. Measurements were performed in triplicates from three independent batches. Transmission electron microscopy (TEM) was performed using a Philips EM208 operating at 60 kV. The suspension of NPs (1 mg.mL⁻¹) was deposited on copper grids covered with a formvar film (400 mesh) for 2 min. Negative staining (30 seconds) with phosphotungstic acid (1%) was performed. The excess solution was blotted off using filter paper and grids were air dried before observation. Image acquisition was performed using a high-resolution camera, Advantage HR3/12GO4 (AMT-Hamamatsu).

Stability studies

NP stability in terms of average diameter, particle size distribution, zeta potential and fluorescence was tested at 4°C in water (storage temperature of the NP suspension) and at 37°C in PBS for several time points. Samples from three independent batches were measured in triplicates. Label stability was investigated by incubating DY-NPs and NPs at 2.5 mg.mL⁻¹ in PBS at 37 °C. At predetermined time intervals (0, 1, 2, 3 and 7 days), samples were ultracentrifuged (maximum 37000 g, 1 h, 4 °C, Beckman Coulter Optima LE-80 K, Beckman Coulter, France) and supernatants were freeze dried (alpha-12-LD, Christ, France). The lyophilisate was then dissolved in DCM and centrifuged for 5 min at 800 × g (MR1812, Jouan, France) to remove PBS salts. The supernatant was then measured in DCM ethanol 2:1 (v:v) fluorimetrically to determine the dye content. Measurements were performed in triplicate for two different batches.

Cell culture and cell viability (MTT assay)

To analyse the impact of labeling on cell viability, three different cell lines were used. Embryonic murine fibroblast (NIH/3T3) and human endothelial umbilical vein cells (HUVEC) were cultured in DMEM supplemented with 50 U.mL⁻¹ penicillin, 50 U.mL⁻¹ streptomycin, and 10% FBS. The J774.A1 murine macrophage-monocyte cell line was cultured in RPMI 1640 medium supplemented with 50 U.mL⁻¹ penicillin, 50 U.mL⁻¹ streptomycin, and 10% heat inactivated FBS. Cells were splitted twice a week, either by trypsinisation for HUVEC and NIH/3T3 cells were trypsinized or by scraping for J774.A1 cells. All cell lines were maintained at 37°C and 5% CO₂ in a humidified atmosphere. In order to evaluate the *in vitro* cytotoxicity, NPs were resuspended in cell culture medium and filtered (PVDF, 0.45 µm) before being added onto the cells. Cell viability was evaluated using the MTT assay as described previously³⁴. Briefly, cells were seeded (8 × 10³ cells/well) in 96-well plates (TPP, Switzerland) and pre-incubated for 24 h. Then, the culture medium was replaced with serial dilutions of NP suspensions or equivalent amounts of pure DY-

700 (n = 14) in culture medium. After 24 h, the incubation medium was replaced by fresh medium containing $0.5 \text{ mg}\cdot\text{mL}^{-1}$ (3-(4,5-dimethylthiazol-2-yl)-2,5-diphenyltetrazolium bromide (MTT) (Sigma, France). After 4 h of incubation, the culture medium was gently aspirated and replaced by 200 μL dimethylsulfoxide (ACS grade, BioBasic Inc, France) to dissolve the formazan crystals. The absorbance of the solubilized dye, which correlates to the number of living cells, was measured with a microplate reader (LAB Systems Original Multiscan MS, Finland) at 570 nm. Cell viability [%] relative to non-treated (control) cells: $[A]_{\text{test}}/[A]_{\text{control}}\times 100$. Polyethyleneimine (PEI) (25 kDa), a cationic polymer, was used as positive control. The IC50 was calculated as the sample concentration which inhibits growth of 50% of cells relative to the control cells according to Unger et al.³⁴. Data are presented as a mean of four measurements \pm standard deviation. IC50 was calculated using the sigmoidal fitting function from Origin® v 8.0 (OriginLab, Northampton, USA) when possible.

Confocal microscopy

The three types of cells were seeded onto glass cover slips (25 mm) inside 6 well plates at a density of 250 000 cells per well with 2 mL of medium and grown for 24 h. Medium was replaced by 2 mL of fresh medium containing NPs ($1 \text{ mg}\cdot\text{mL}^{-1}$) and incubated at 37°C for further 24 h. Then, the medium was gently removed and the cover slips were covered with 1 mL of fresh medium and analysed using a confocal laser scanning microscope LSM 510 META (Zeiss, Germany) equipped with a 1mW Helium Neon Laser and a Plan-Apochromat 63X objective lens (Numerical Aperture 1.40, oil immersion) coupled with an LSM 5 Image Browser (Zeiss, Germany). The cover slips were maintained at 37°C during image acquisition. Red fluorescence was observed with a 650 nm long pass emission filter under a 633 nm laser illumination.

Fluorescence Reflectance Imaging (2D-FRI)

Imaging of mice was performed as described previously^{14, 35}. All animal experiments were performed in agreement with the EEC guidelines and the Principles of laboratory animal care (NIH publication 14, No. 86-23, revised 1985). The investigator (L.S.) possesses the authorization number 38-09-22. Female NMRI nude mice (6 weeks old, n = 14, Janvier, Le Genest-Saint-Isle, France) were used and randomly separated into six different groups. Anesthetized mice (isoflurane/oxygen 3.5/4% for induction and 1.5/2% thereafter, CSP, Cournon, France) were injected intravenously with 200 μL of $25 \text{ mg}\cdot\text{mL}^{-1}$ NPs or equivalent dye concentration alone (n = 3 mice/group), $5 \text{ mg}\cdot\text{mL}^{-1}$ NPs or equivalent dye concentration alone (n = 3 mice/group) or $1 \text{ mg}\cdot\text{mL}^{-1}$ NPs or equivalent dye concentration alone (n = 1 mouse/group). NP suspensions were filtered on a 0.45 μm PVDF filter prior to injection. Mice were illuminated by 675 nm light-emitting diodes

equipped with interference filters and emission was collected by 720/20 nm pass-band filter (IVIS Kinetic, Caliper, Villepinte, France). Fluorescence images were acquired during 1 sec at 90 min, 3 h, 5 h (n = 3 mice/group) and 24 h (n = 1 mouse/group) after injection. At the end of the experiment, 5 h or 24 h after injection, mice were euthanized to visualize the *ex vivo* fluorescence in the different organs (heart, lung, brain, skin, muscle, kidney, adrenal, bladder, intestine, spleen, pancreas, fat, stomach, uterus/ovary and liver).

Results and Discussion

DY-700 amine, a hemicyanine dye, was chosen for the conjugation to PLGA due to its characteristics in the NIR range and its primary amine group which allows a convenient coupling reaction (Figure 1, inset). The absorption spectrum of DY-700 amine in DCM:ethanol 2:1 (v:v) presents a maximum at 700 nm, a shoulder around 650 nm and an additional maximum in the visible range at 485 nm. When excited at 700 nm the emission maximum is situated at 725 nm (Figure 1). These absorption/emission characteristics are similar in water and in serum. Besides from being used for NIR animal experiments, it also allows visualization *in vitro* for example by confocal laser microscopy due to these fluorescence characteristics.

For the sake of simplicity, we propose a 2 step–one pot functionalization strategy whereby the PLGA is end-functionalized with a NHS moiety using DCC/NHS and further reacted *in situ* with the amino NIR dye (Figure 2a). The carboxylic acid group of PLGA RG502 H was activated *via* DCC/NHS and the resulting PLGA was reacted *in situ* with the amino group of the DY-700 in a DMF:DCM mixture. The synthesis *via* NHS activated ester avoids intramolecular and intermolecular esterification between hydroxyl and carboxylic acid groups of PLGA³⁶. To ensure purification was complete, several precipitation/centrifugation cycles were performed and supernatants were monitored *via* fluorimetry. The precipitate was dark green proving the effective linkage. Indeed, the fluorescent spectrum of the DY-PLGA in DCM:ethanol 2:1 (v:v) is identical to the spectrum of the DY-700 amine (Supplementary material, Figure S1). It appears that 4 precipitation/centrifugation cycles were sufficient to remove unreacted dye, allowing a 92% yield to be obtained. Fluorimetry shows that the labeling efficacy was 38%, which is about 4-fold higher than what was obtained by Tosi et al.²⁰ Given the molecular weights of DY-700 (747 g.mol⁻¹) and of PLGA RG502 H (M_n 7900 g.mol⁻¹, M_w 14600 g.mol⁻¹), DY-PLGA therefore contains 3.5% DY-700 (w/w). The conjugate was also analyzed via SEC. DY-PLGA presents an intense signal at 485

nm which overlaps with its RI signal whereas PLGA does not show any signal at 485 nm, which proves the successful covalent coupling of the dye to PLGA (Figure 2b).

PLGA NPs were then formulated replacing 1% of PLGA RG756 S by DY-PLGA conjugate. In the following, the resulting fluorescent NPs will be noted DY-NPs whereas the non-fluorescent counterparts will be noted NPs. A DY-NP suspension of 1 mg.mL^{-1} therefore corresponds to an equivalent dye concentration of $0.35 \text{ }\mu\text{g.mL}^{-1}$. DY-NP fluorescence in water gives the same spectrum as the DY-PLGA in DCM:ethanol 2:1 (v:v) (Supplementary material, Figure S1). DY-NPs were characterized and compared to NPs (Table 1). All NPs present average diameters between 205 and 220nm with a monomodal size distribution and a low polydispersity (PDI below 0.2) and slightly negative zeta potentials, independently of the presence of DY-PLGA conjugate. TEM images confirm that particles are spherical, rather monodisperse and around 200nm (Figure 3b, inset). The absence of modifications has already been observed for rhodamine B-labeled PLGA NPs³⁷. In addition, incorporation of 1% of DY-PLGA conjugate hardly affects size, PDI and zeta potential either before or after centrifugation, when redispersed at 5 mg.mL^{-1} and 25 mg.mL^{-1} . Moreover, XPS spectra of NPs and DY-NPs are identical (data not shown): the absence of modifications after incorporation of the NIR conjugate further confirms that down to 10 nm thickness, the surface chemistry of DY-NPs does not differ from NPs. Therefore, the *in vivo* fate of DY-NPs after intravenous administration can be assumed to be identical to the fate of NPs.

According to our calculations, 1% DY-PLGA for labeling was chosen as a balance between fluorescence emission and dye self-quenching. Since DY-NPs are prepared using 24.75 mg PLGA and 0.25 mg DY-PLGA, one formulation therefore contains 7.05×10^{15} labels for an available surface of a 0.505 m^2 (PLGA density = 1.35 g.cm^{-3} , NP radius = 110 nm). Assuming that all dyes are positioned at the surface of DY-NPs, the available surface for each label is 71.6 nm^2 , which corresponds to an average distance of 17 nm between each fluorescent molecule. This is larger than the Förster radius that is above 6 nm for cyanine dyes³⁸. The fluorescence intensities of the dye and of the DY-NPs for equivalent dye concentrations were compared as a function of NP concentration (Figure 3), both in water or in serum. Since DY-700 is not very soluble in water or aqueous buffer and tends to precipitate, fluorescence of DY-NPs in water is much higher than the one provided by an equivalent concentration of DY-700. Indeed, the linkage of DY-700 on NP surface prevents self-aggregation of the DY-700 molecules. This kind of behavior has been described for other NIR dye conjugated systems such as fluorescent silica NPs or fluorescent probes with proteins^{39, 40}. In serum, the fluorescence of the DY-700 is much higher than in water. The presence of proteins containing hydrophobic domains enhances the solubility of the dye and might prevent its

aggregation. This effect has been described for cyanine dyes in bovine serum albumin solution³⁹. There is no difference of fluorescence intensity between DY-NPs in water or in serum. Importantly, one should notice that the fluorescence intensity of the DY-NPs or the dye itself in serum were comparable. Therefore for *in vivo* experiments, we chose to use the equivalent dye concentration when comparing with DY-NPs.

Stability of NPs and DY-NPs was tested at 4°C (Figure 4). Both types of NPs exhibit a strong storage stability over a month. Size and zeta potentials remained stable and PDIs were below 0.1. Good storage stability facilitates studies as NPs do not have to be produced directly prior to their use. In addition, fluorescence was also monitored over a month at 4°C at different concentrations, measuring the very same samples repeatedly (Figure 5). Different NP concentrations were used to take into account the slight quenching observed at high concentration. No significant fluorescence decrease occurred over a month.

Stability was then investigated in PBS buffer at 37°C over a week. The concentrations of 2.5 and 0.5 mg.mL⁻¹, that correspond to 1/10 dilution that should occur after NP intravenous injection in mice, show very good stability with no modification of the colloidal characteristics. The lowest concentration 0.1 mg.mL⁻¹ seems less stable with a slight increase of the PDI which however remained below 0.2 until the third day. At this high dilution, the increase of polydispersity may arise from a removal of the PVA layer stabilizing nanoparticles. Stability was also assessed in cell culture media and in serum over 24 h during which particle size remain stable. The good NP stability in all tested media provides a proof of the absence of aggregation, and anticipates what would happen when NPs *in vitro* on cells or *in vivo* in mice. One the main advantage of covalently labeling of the polymer is that it avoids dye leakage that could produce artifacts^{21, 22}. The stability of the labeling was verified by incubating DY-NPs in PBS at 37°C over a week. Figure 6 shows that only 2.5% of the label is released over week, proving the good stability of the conjugate.

Before *in vivo* evaluation, NP cytotoxicity was assessed *in vitro* for three different cell lines (Figure 7). Free dye was also tested at equivalent concentrations found in DY-NPs. For HUVEC cells, a human umbilical vein endothelial cell line, and NIH/3T3, a mouse embryonic fibroblast cell line, cell viability remains above or around 50% for both NPs and DY-NPs and the IC₅₀ cannot be determined. The cell viability was very slightly affected by the dye itself even at dye concentrations up to 7 µg.mL⁻¹. In J774.A1, a murine macrophage-like cell line, cell viability decreases as a function of NP concentration. The IC₅₀ is ~35-40 µg.mL⁻¹ for both NPs and DY-NPs. Interestingly, the cell viability decreases quickly after the IC₅₀ concentration, but remains around

30 % between 0.25 and 1 mg.mL⁻¹. Incubation of J774.A1 with the free dye leads to a decrease of cell viability around 80% for dye concentration up to 7 µg.mL⁻¹. These different toxicity profiles may arise from differences in the type of cells, as a macrophage-like cell line would probably take up particles much more actively than other cell types. In addition, apart from macrophages, many cell types do not internalize neutral particles in large quantities as they show only limited interaction with the cell membrane⁴¹. To verify this hypothesis, DY-NP uptake was visualized with confocal laser microscopy. HUVEC and NIH/3T3 cells indeed do not seem to significantly internalize DY-NPs. On the other hand, J774.A1 cells actively internalize DY-NPs due to their well-known tendency for endocytosis. These observations confirm cytotoxicity results. NPs remain in the cytoplasm and do not seem to enter the nucleus.

DY-NPs and equivalent concentrations of free dye were then injected intravenously to mice (Figure 9 and 10). *In vivo*, fluorescence can be observed in the guts, arising from autofluorescent food. A difference in fluorescence distribution can be observed quickly after injection. The dye, which is a low molecular weight compound, shows a much faster clearance, whereas DY-NPs are found more importantly in the liver. Indeed, as DY-NPs were not PEGylated NPs (i.e., stealth), they were quickly opsonized and recognized by macrophages and ended-up in organs of the MPS such as liver, bone marrow and spleen⁴². This result is confirmed by the evaluation of the fluorescence intensity of the different organs *ex vivo* 5 h after injection. A higher fluorescent signal is recovered from the spleen and the liver for DY-NPs than for the dye itself, whereas the levels of fluorescence are comparable for other organs (Figure 10, top). Evaluation of the *ex vivo* fluorescence of the liver confirms this tendency 24 h hours after injection and for the different concentrations injected (Figure 10, bottom). In addition, after 24 h, the liver fluorescence decreased as compared with the 5 h time point, indicating that clearance has started (Figure 10, bottom). Importantly, these NPs exhibit intense fluorescence signal *in vivo* after intravenous administration using as low as 1 % DY-PLGA conjugate in the NP formulation, which allow them to be finely traced.

Conclusion

We have successfully synthesized a covalent conjugate of PLGA with a NIR dye (DY-700, Dyomics) with 38 % coupling efficiency, using DCC/NHS chemistry. The conjugate was incorporated at 1% (w/w) into PVA-stabilized PLGA NPs without modifying major NP features such as size, zeta potential, stability and cytotoxicity on HUVEC, NIH/3T3 or J774.A1 cell cultures. The absence of modifications after incorporation of the NIR conjugate further confirms that the surface chemistry of DY-NPs does not differ from NPs. Therefore, the *in vivo* fate of DY-

NPs after intravenous administration can be assumed to be identical to the biodistribution of NPs. *In vivo*, after intravenous injection to nude mice, DY-NPs fate was followed down to concentrations of 1 mg.mL⁻¹. NP accumulation in the liver was easily monitored by NIR imaging providing a proof of concept for *in vivo* tracking the fate of PLGA-based nanosystems using the DY-PLGA conjugate at rather low concentration.

Acknowledgements

Authors would like to acknowledge B. Le Droumaguet and N. Mackiewicz for fruitful discussions, V. Nicolas (IPSIT, Univ Paris-Sud, Châtenay Malabry) for confocal experiments, S. Zanna (Chimie Paris Tech) for XPS analysis, D. Jaillard (CCME, Orsay, Univ Paris-Sud) for TEM, M. Henry for animal experiments and R. Skanji for help collecting rat serum. This study was supported by AFSSET (“Emerging risks” program) and by ANR (under reference 2009-CESA-011). R. Reul and S. Mura acknowledge the support of ANR for their fellowship.

References

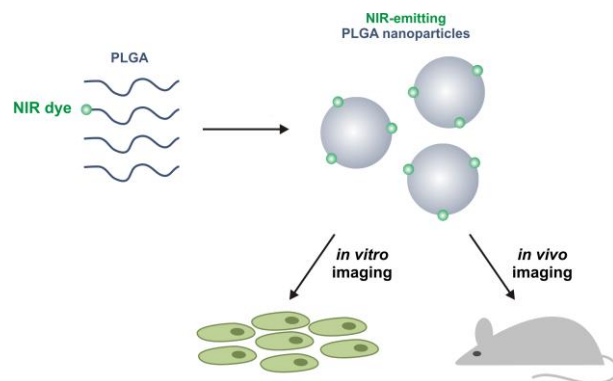
1. G. Gaucher, R.H. Marchessault, and J.C. Leroux, *J Control Release*, 2010, **143**, 2-12.
2. I. Bala, S. Hariharan, and M.N. Kumar, *Crit Rev Ther Drug Carrier Syst*, 2004, **21**, 387-422.
3. E. Pisani, N. Tsapis, B. Galaz, M. Santin, R. Berti, N. Taulier, E. Kurtisovski, O. Lucidarme, M. Ourevitch, B.T. Doan, J.C. Beloeil, B. Gillet, W. Urbach, S.L. Bridal, and E. Fattal, *Adv Funct Mater*, 2008, **18**, 2963-2971.
4. A. Kumari, S.K. Yadav, and S.C. Yadav, *Colloids and Surfaces B: Biointerfaces*, 2010, **75**, 1-18.
5. R. Duffin, C.L. Tran, A. Clouter, D.M. Brown, W. MacNee, V. Stone, and K. Donaldson, *Ann Occup Hyg*, 2002, **46**, 242-245.
6. G. Oberdorster, E. Oberdorster, and J. Oberdorster, *Environ Health Perspect*, 2005, **113**, 823-839.
7. K. Wittmaack, *Environ Health Perspect*, 2007, **115**, 187-194.
8. K. Donaldson, R. Aitken, L. Tran, V. Stone, R. Duffin, G. Forrest, and A. Alexander, *Toxicological Sciences*, 2006, **92**, 5-22.
9. R. Fernandez-Urrusuno, E. Fattal, D. Porquet, J. Feger, and P. Couvreur, *Toxicol Appl Pharmacol*, 1995, **130**, 272-279.
10. R. Kumar, I. Roy, T.Y. Ohulchanskyy, L.A. Vathy, E.J. Bergey, M. Sajjad, and P.N. Prasad, *ACS Nano*, 2010, **4**, 699–708.
11. S. Wiegand, T. Heinen, A. Ramaswamy, A.M. Sesterhenn, C. Bergemann, J.A. Werner, and A.S. Lubbe, *J Drug Target*, 2009, **17**, 194-199.
12. A. Ashokan, D. Menon, S. Nair, and M. Koyakutty, *Biomaterials*, 2010, **31**, 2606-2616.
13. E.I. Altinoglu and J.H. Adair, *Wiley Interdiscip Rev Nanomed Nanobiotechnol*, 2010.
14. S. Dufort, L. Sancey, C. Wenk, V. Josserand, and J.L. Coll, *Biochimica et Biophysica Acta (BBA) - Biomembranes*, 2010, **1798**, 2266-2273.
15. J. Rao, A. Dragulescu-Andrasi, and H. Yao, *Curr Opin Biotechnol*, 2007, **18**, 17-25.
16. B.J. Nehilla, P.G. Allen, and T.A. Desai, *ACS Nano*, 2008, **2**, 538-544.
17. J. Pan and S.S. Feng, *Biomaterials*, 2009, **30**, 1176-1183.
18. J. Nicolas, D. Brambilla, O. Carion, T. Pons, I. Maksimovic, E. Larquet, B. Le Droumaguet, K. Andrieux, B. Dubertret, and P. Couvreur, *Soft Matter*, 2011, **7**, 6187-6193.

19. J.S. Kim, K.J. Cho, T.H. Tran, M. Nurunnabi, T.H. Moon, S.M. Hong, and Y.K. Lee, *J Colloid Interface Sci*, 2011, **353**, 363-371.
20. G. Tosi, L. Bondioli, B. Ruozi, L. Badiali, G.M. Severini, S. Biffi, A. De Vita, B. Bortot, D. Dolcetta, F. Forni, and M.A. Vandelli, *J. Neural Transm.*, 2011, **118**, 145-153.
21. P. Pietzonka, B. Rothen-Rutishauser, P. Langguth, H. Wunderli-Allenspach, E. Walter, and H.P. Merkle, *Pharm Res*, 2002, **19**, 595-601.
22. P. Xu, E. Gullotti, L. Tong, C.B. Highley, D.R. Errabelli, T. Hasan, J.X. Cheng, D.S. Kohane, and Y. Yeo, *Mol Pharm*, 2009, **6**, 190-201.
23. Y.C. Huang, Y.Y. Huang, C.C. Huang, and H.C. Liu, *J Biomed Mater Res B Appl Biomater*, 2005, **74**, 659-664.
24. J. Panyam, W.Z. Zhou, S. Prabha, S.K. Sahoo, and V. Labhasetwar, *FASEB J*, 2002, **16**, 1217-1226.
25. J.P. Bertram, S.M. Jay, S.R. Hynes, R. Robinson, J.M. Criscione, and E.B. Lavik, *Acta Biomater*, 2009, **5**, 2860-2871.
26. A. Besheer, J. Vogel, D. Glanz, J. Kressler, T. Groth, and K. Mader, *Mol Pharm*, 2009, **6**, 407-415.
27. M. Bivas-Benita, S. Romeijn, H.E. Junginger, and G. Borchard, *Eur J Pharm Biopharm*, 2004, **58**, 1-6.
28. H. Chen, W. Yang, L. Liu, F. Gao, X. Yang, Q. Jiang, Q. Zhang, and Y. Wang, *Colloids Surf B Biointerfaces*, 2009, **73**, 212-218.
29. J. Cheng, B.A. Teply, I. Sherifi, J. Sung, G. Luther, F.X. Gu, E. Levy-Nissenbaum, A.F. Radovic-Moreno, R. Langer, and O.C. Farokhzad, *Biomaterials*, 2007, **28**, 869-876.
30. R. Diaz-Lopez, N. Tsapis, M. Santin, S.L. Bridal, V. Nicolas, D. Jaillard, D. Libong, P. Chaminade, V. Marsaud, C. Vauthier, and E. Fattal, *Biomaterials*, 2010, **31**, 1723-1731.
31. E.B. Lavik, J.S. Hrkach, N. Lotan, R. Nazarov, and R. Langer, *J Biomed Mater Res*, 2001, **58**, 291-294.
32. C. Gomez-Gaete, N. Tsapis, M. Besnard, A. Bochot, and E. Fattal, *Int J Pharm*, 2007, **331**, 153-159.
33. C. Gomez-Gaete, E. Fattal, L. Silva, M. Besnard, and N. Tsapis, *J Control Release*, 2008, **128**, 41-49.
34. F. Unger, M. Wittmar, and T. Kissel, *Biomaterials*, 2007, **28**, 1610-1619.
35. Z.H. Jin, V. Josserand, S. Foillard, D. Boturyn, P. Dumy, M.C. Favrot, and J.L. Coll, *Mol Cancer*, 2007, **6**, 41.
36. G.W. Cline and S.B. Hanna, *J. Am. Chem. SOC.*, 1987, **109**, 3087-3091
37. S. Mura, H. Hillaireau, J. Nicolas, B. Le Droumaguet, C. Gueutin, S. Zanna, N. Tsapis, and E. Fattal, *Int J Nanomedicine*, 2011, **6**, 2591-2605.
38. A.A. Deniz, M. Dahan, J.R. Grunwell, T.J. Ha, A.E. Faulhaber, D.S. Chemla, S. Weiss, and P.G. Schultz, *P Natl Acad Sci USA*, 1999, **96**, 3670-3675.
39. P. Czerney, F. Lehmann, M. Wenzel, V. Buschmann, A. Dietrich, and G.J. Mohr, *Biol Chem*, 2001, **382**, 495-498.
40. E. Herz, H. Ow, D. Bonner, A. Burns, and U. Wiesner, *J. Mater. Chem.*, 2009, **19**, 6341-6347
41. A.F. Adler and K.W. Leong, *Nano Today*, 2010, **5**, 553-569.
42. D. Bazile, C. Prud'homme, M.T. Bassoulet, M. Marlard, G. Spenlehauer, and M. Veillard, *J Pharm Sci*, 1995, **84**, 493-498.

Tables and Figures

Table 1: Average diameters, Polydispersity Index (PDI) and Zeta Potential of NPs and DY-NPs before and after centrifugation at 5 and 25 mg.mL⁻¹. Data are presented as mean \pm SEM.

Nanoparticles		Average Diameter (nm)	PDI	Zeta potential (mV)
Before centrifugation	NP	206 \pm 11	0.035 \pm 0.02	- 4.9 \pm 0.5
	DY-NP	213 \pm 6	0.062 \pm 0.026	- 4.3 \pm 0.5
After centrifugation	NP 5 mg.mL ⁻¹	207 \pm 5	0.048 \pm 0.024	- 4.5 \pm 0.6
	DY-NP 5 mg.mL ⁻¹	214 \pm 2	0.039 \pm 0.002	- 5.1 \pm 0.4
	NP 25 mg.mL ⁻¹	218 \pm 2	0.190 \pm 0.069	- 4.5 \pm 0.2
	DY-NP 25 mg.mL ⁻¹	219 \pm 4	0.140 \pm 0.064	- 4.8 \pm 0.3



Scheme 1: Synthesis of NIR-emitting PLGA nanoparticles and their used for *in vitro*, *in vivo* and *ex vivo* imaging purposes.

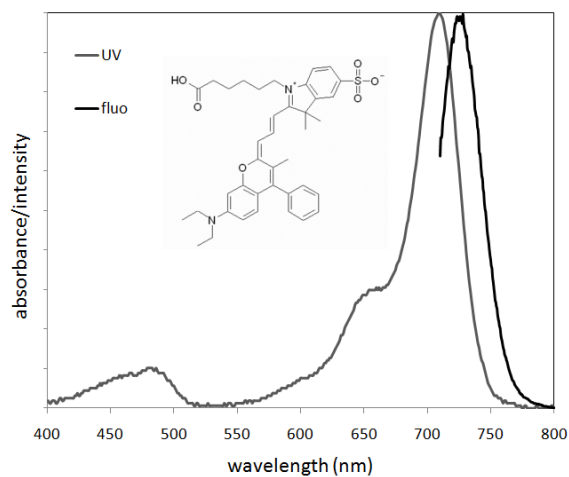


Figure 1: Fluorescence and UV spectrum of DY-700 amine in DCM:ethanol 2:1 (v:v). The inset presents the chemical structure of the precursor of DY-700 amine NIR dye.

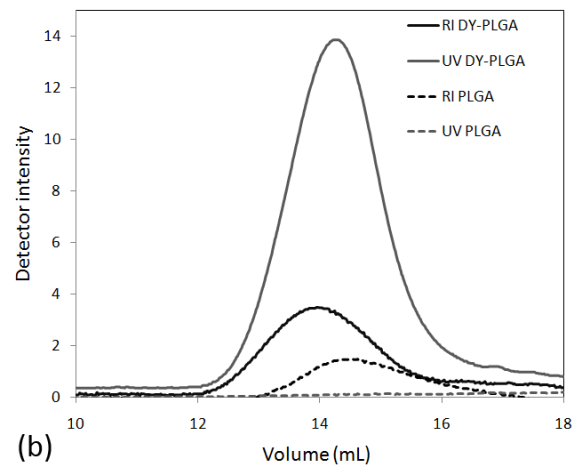
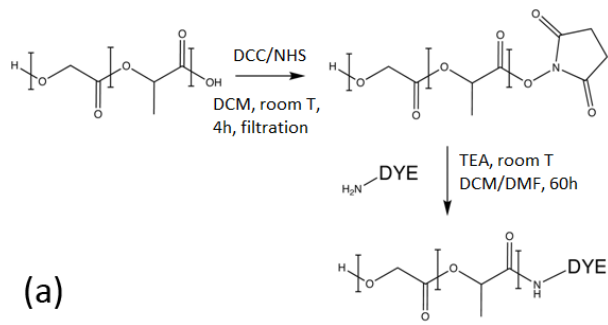


Figure 2: Synthesis scheme of the DY-PLGA conjugate (a) and SEC chromatogram of PLGA and DY-PLGA (b).

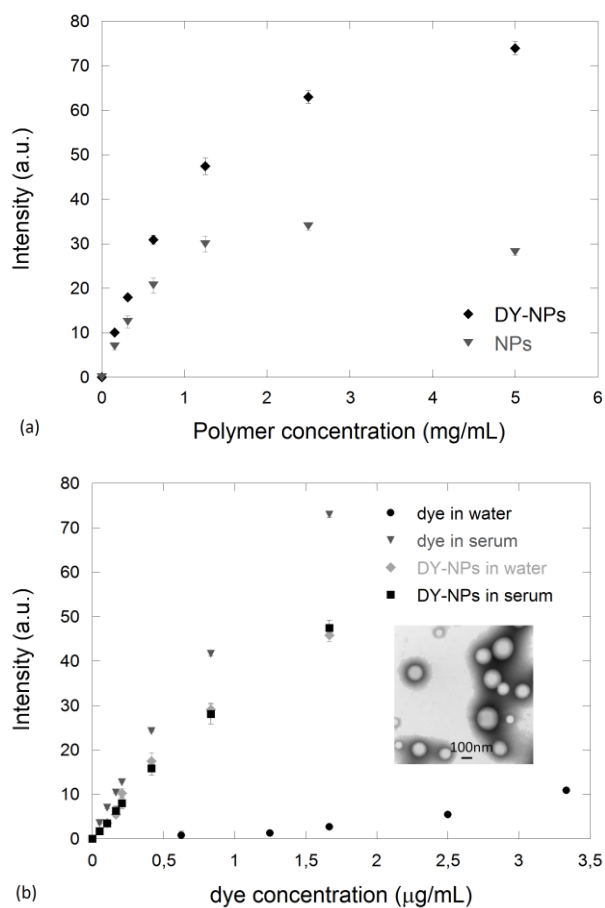


Figure 3: Fluorescence characterization of the nanoparticles. Fluorescence intensity ($\lambda_{\text{ex}}=700$ nm, $\lambda_{\text{em}}=725$ nm) of DY-NPs in comparison with NPs (a). DY-NP fluorescence corrected by the effect of NPs in comparison with pure dye expressed in dye concentration, in water and in serum (b). The inset in (b) presents a typical TEM image of the DY-NPs. Data are presented as mean \pm SEM.

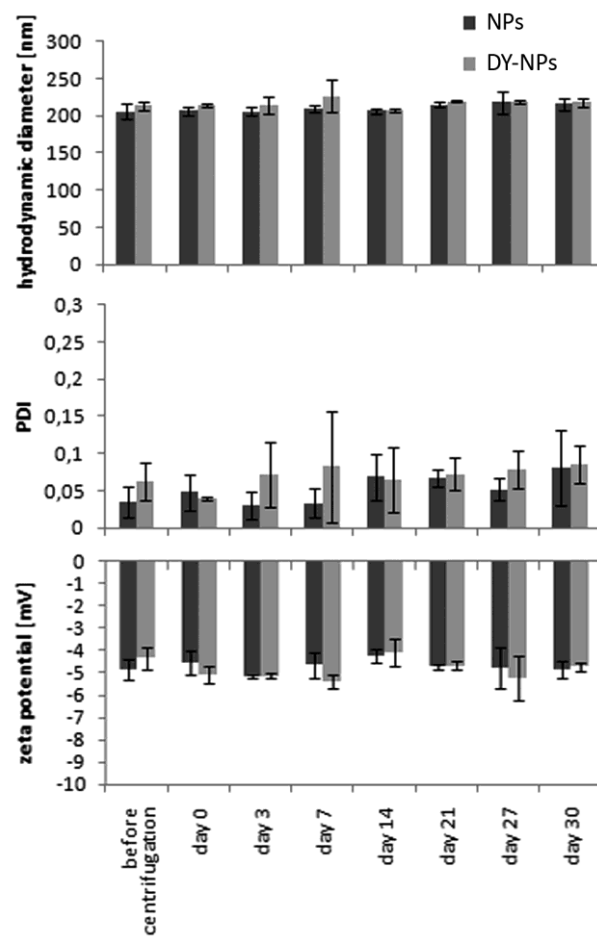


Figure 4: Stability of NPs and DY-NPs (5 mg.mL^{-1}) at 4°C over 30 days: Top: Average diameter, Middle: PDI, Bottom: Zeta potential. Data are presented as mean \pm SEM.

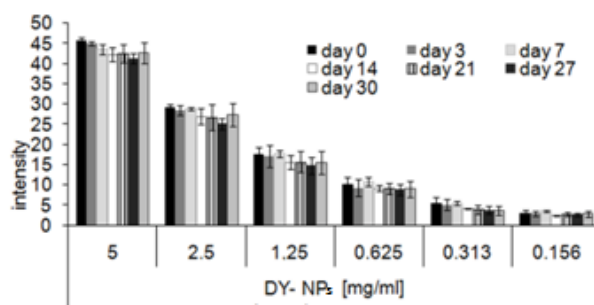


Figure 5: Fluorescence stability of DY-NPs at 4°C at different concentrations (fluorescence intensity corrected from NP fluorescence). Data are presented as mean \pm SEM.

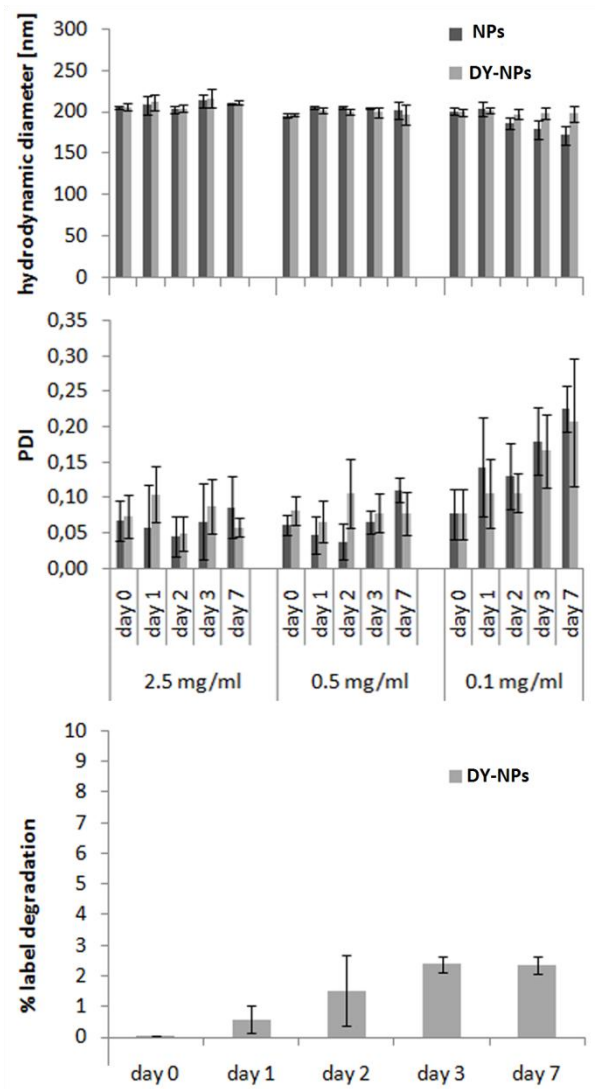


Figure 6: NPs and DY-NPs stability at 37°C in PBS over a week. Top: Average diameter, Middle: PDI, Bottom: Label degradation. Data are presented as mean ± SEM.

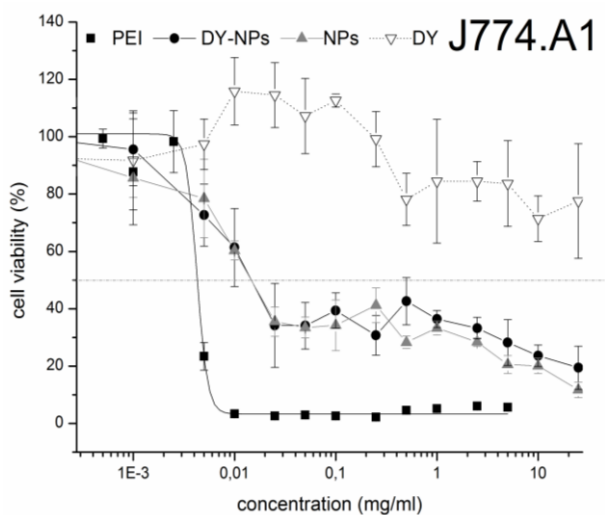
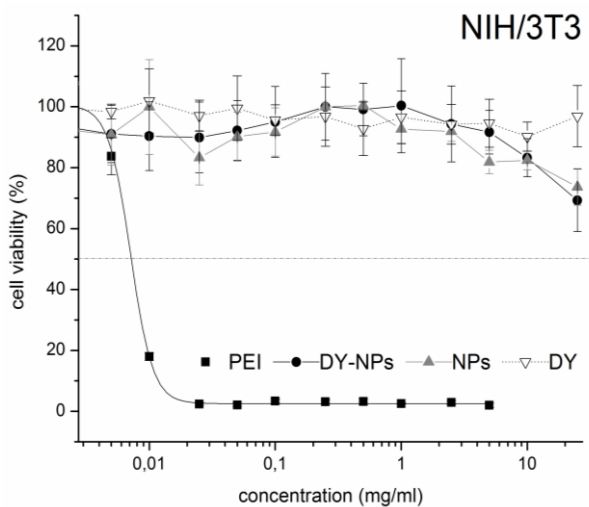
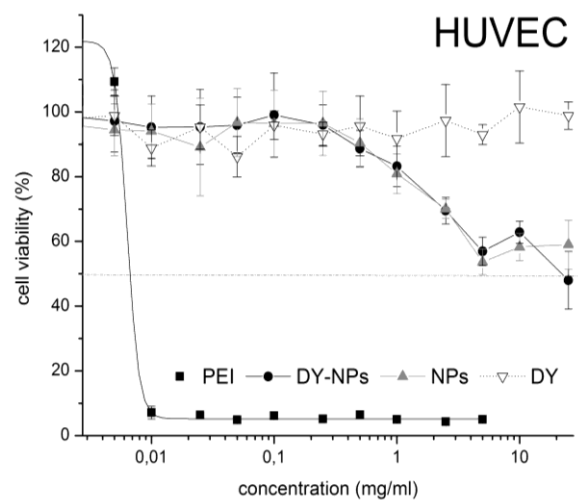


Figure 7: Cell viability as a function of concentration DY-NPs, NPs, equivalent dye concentrations (1mg/mL DY-NPs corresponds to 0.35 μg/mL dye) and PEI as control. Top: HUVEC, Middle: NIH/3T3 and Bottom: J774.A1. PEI results are fitted by a sigmoidal curve. Data are presented as mean ± SD.

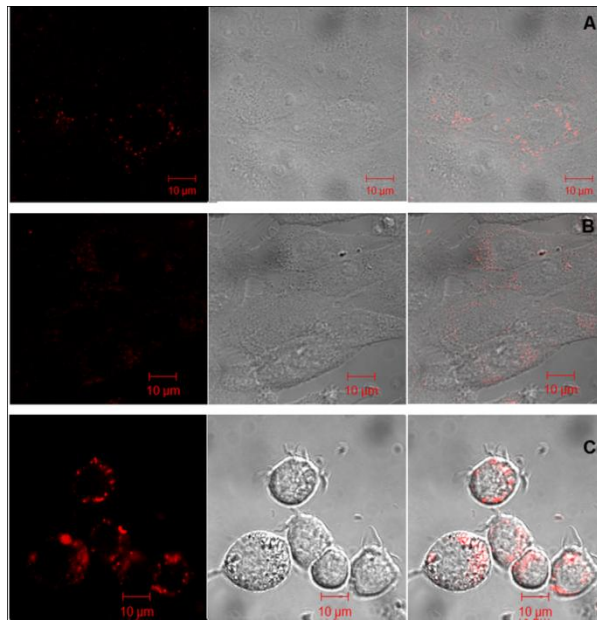


Figure 8: CLSM (left), Nomarsky (center) and merge (right) images of 1 mg.mL^{-1} of DY-NPs incubated with A) HUVEC, B) NIH/3T3 and C) J774.A1.

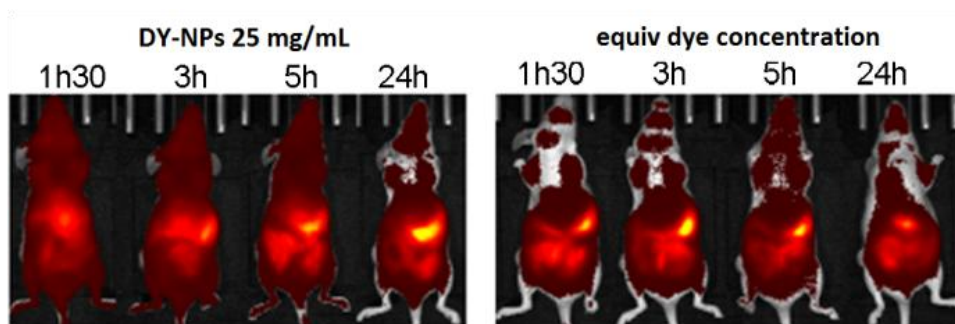


Figure 9: *In vivo* NIR images of DY-NPs (left) and equivalent concentration of free dye (right) in nude mice as a function of time.

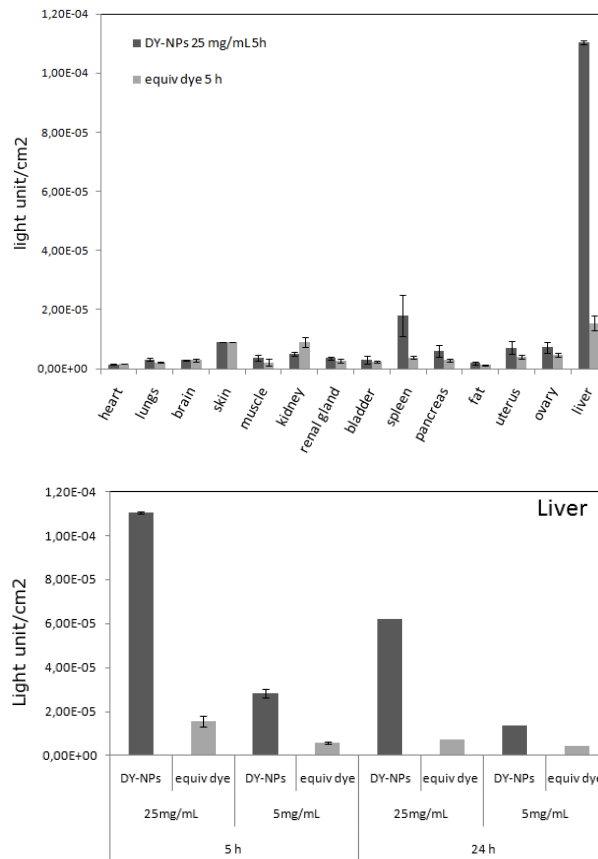


Figure 10: *Ex vivo* organ distributions of DY-NPs and equivalent amounts of pure DY in nude mice measured by NIR 5 h post-injection. Top: all organs, Bottom: liver 5 and 24 hours post-injection. Data are presented as mean \pm SEM.